

EM Implosion Memos

Memo 35

October 2009

Numerical simulations of a 60° four-feed-arm PSIRA to determine the beam width inside a focusing lens

Prashanth Kumar, Carl E. Baum, Serhat Altunc, Christos G. Christodoulou and Edl Schamiloglu

University of New Mexico

Department of Electrical and Computer Engineering

Albuquerque, NM 87131

Abstract

This paper presents the numerical simulation results of a 60° four feed-arm PSIRA with a focusing lens. Observations are made on the focal waveform inside the lens. The beam width inside the focusing lens is compared to the beam width in air (without the lens). The focal waveforms and beam widths are compared to analytical approximations in [1]. Some additional notes are made on the focal waveforms inside the lens and in air.

1 Introduction

Theoretical considerations in [2] are based on a simple model with a step rising input, i.e., the input has 0 rise time. The model does not take into account the sphericity of the hemispherical focusing lens and the number of feed arms. In our experiments, the 60° four feed arm configuration is used due to the higher electric fields obtained at the focus, compared to the two arm and 45° four arm cases [3, 4]. The scaling relationships in [1] provide insight into the scaling of fields at the focal point but are not applicable to distances away from the focal point. Also, results in [1] do not provide information on the beam width (spot size). Numerical simulations with less assumptions, which take into account the complete problem, are therefore required to provide more realistic and accurate results.

In this paper, the electric and magnetic field waveforms, at the second focal point, in air and inside the focusing lens, are presented. The electric and magnetic field spot sizes (beam widths), in air and inside the lens, are compared.

2 Setup

2.1 Structure visualization

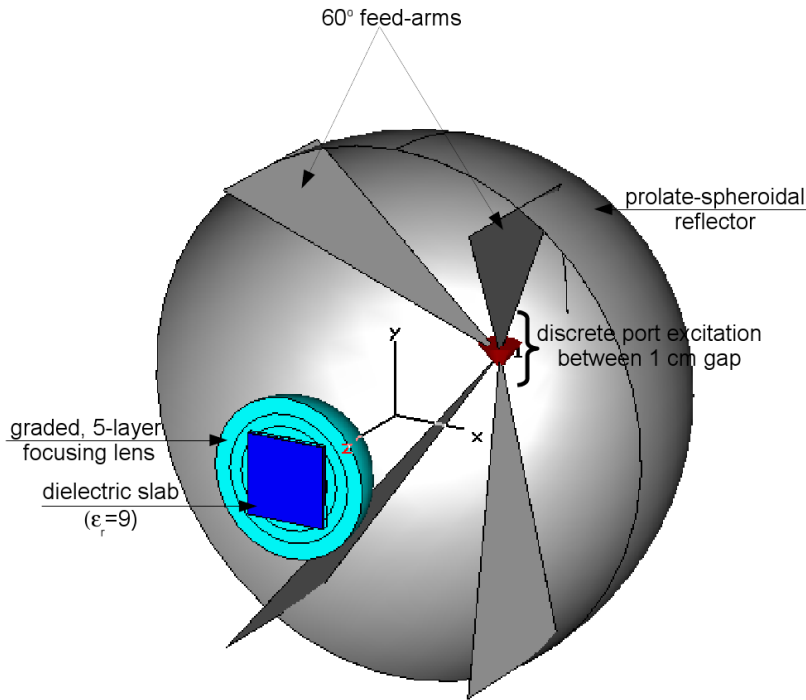


Figure 2.1: Simulation setup of full system with a prolate-spheroidal reflector, four feed-arms at 60° , the hemispherical 5-layer focusing lens and a slab ($\epsilon_r = 9.0$).

The simulation setup of the full system is shown in Fig. 2.1. As seen, it consists of the prolate-spheroidal reflector and four feed-arms at 60° . The hemispherical 5-layer focusing lens shown in the figure has its center at the second focal point. The slab in front of the focusing lens is used as

a “target” medium to impedance match the spherical wave converging at the second focal point in the lens. The slab is included to replicate the experimental setup used to make measurements. A discrete port excitation is applied between a 1 mm gap in the feed arms. The setup to obtain electric and magnetic field beam widths in air is identical to Fig. 2.1, without the focusing lens and the slab.

2.2 Probe placements

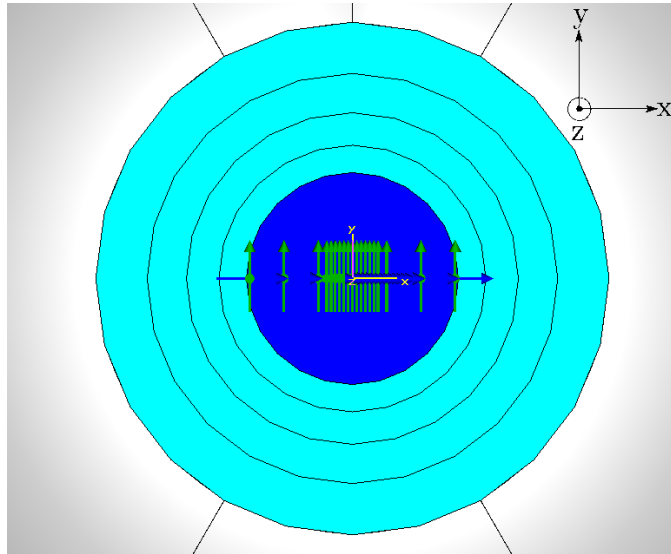


Figure 2.2: Electric field probe placements along the x -axis from the focal point outwards.

Electric field probe placements are shown in Fig. 2.2. Probes were placed along the x -axis, where $x = 0$ cm corresponds to the focal point. Probes were placed at $|x| = 0, 0.25, 0.5, 1.0, 1.25, 1.5, 2.0, 4.0$ and 6.0 cm oriented along $+y$. The magnetic field probes were placed at the same locations and oriented along $+x$. Both the electric and magnetic fields are on the xy -plane.

2.3 Field monitors

2D/3D electric and magnetic field xy -plane field monitors were placed at the second focal point. These planes are used to obtain information on the time evolution of the EM fields.

2.4 Important CST/Simulation Parameters

Domain	Time
Excitation	Discrete
Input	Ramp rising with 100 ps rise time
Excitation voltage	1 V
Frequency range	0–10 GHz
LPW	10

3 Results

3.1 3D electric and magnetic fields

The 3D view of the maximum electric field at the second focal point is shown in Fig. 3.1.

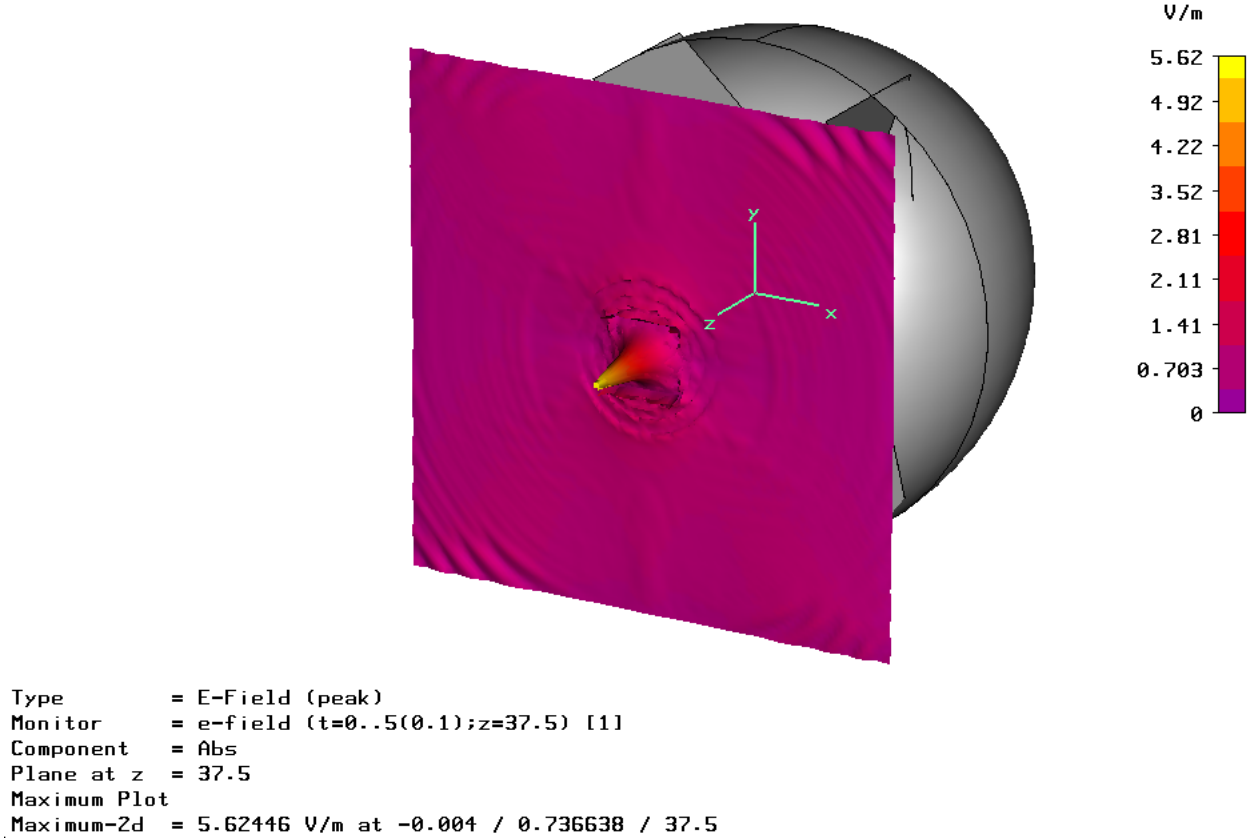
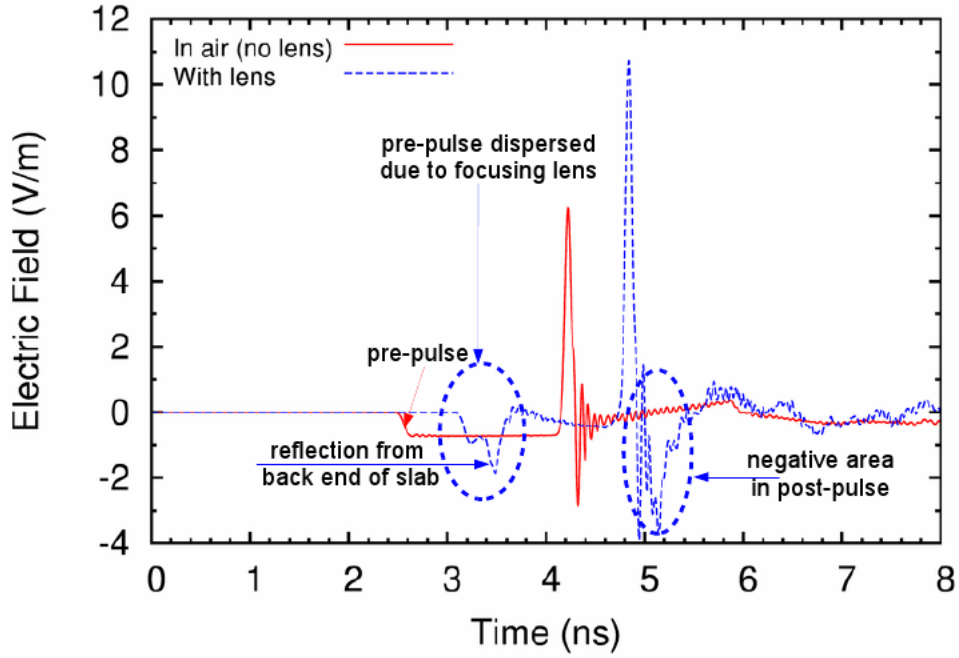


Figure 3.1: 3D view of maximum electric field at second focal point

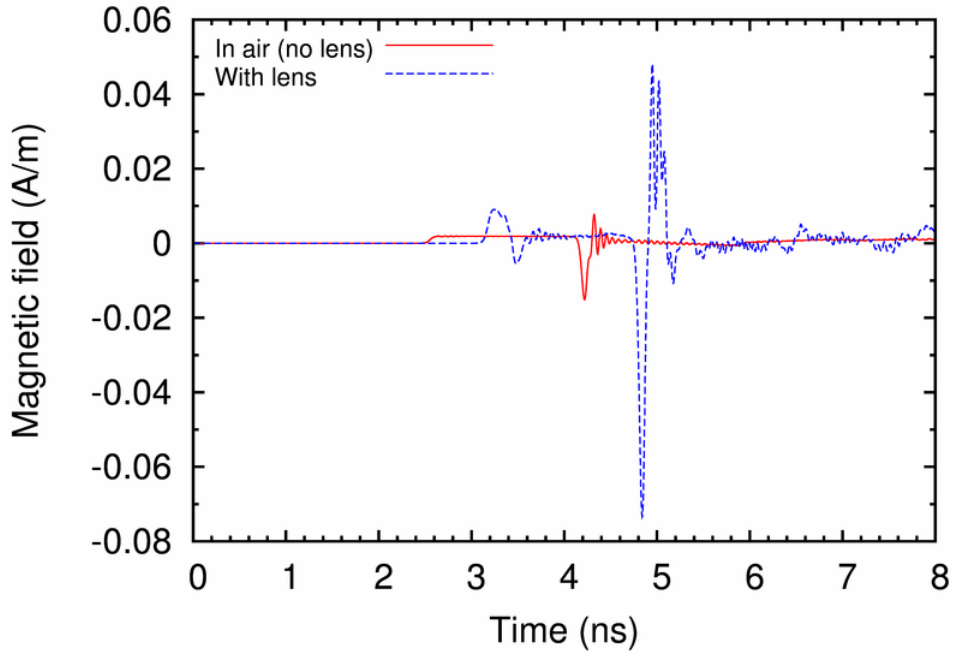
3.2 Observations on the focal waveform

The pre-pulse, impulse and post-pulse responses at the focal point, for the electric and magnetic fields, in air and in the lens, are shown in Fig. 3.2. The observations made here are only for the electric field, although they are applicable to results for the magnetic field.

With reference to Fig. 2(a), one notes that with the lens and slab, the pre-pulse is *dispersed*. A second minimum, occurring immediately after the pre-pulse, is due to the (round-trip) reflection from the slab. The electric enhancement, inside the lens, is approximately $10.725/6.247 = 1.717 \approx \epsilon_r^{1/4} = 9.0^{1/4}$, as calculated in [1]. The negative area under the post-pulse, with the lens, is due to the low frequencies filtered by the focusing lens. The lens and slab materials are assumed dispersionless and lossless in the simulations. Therefore, the filtering action is most likely due to the geometry of the lens itself. The magnetic enhancement, Fig. 2(b), is approximately $0.0734/0.0151 = 4.85 \approx \epsilon_r^{3/4} = 9.0^{3/4}$ as estimated in [1].



(a) Front view



(b) Top view

Figure 3.2: Comparison of the electric and magnetic field responses at the focal point with and without the focusing lens and slab

Important electromagnetic parameters and their scaling relationships, as obtained from Fig. 3.2, are tabulated in Table 1. These results agree very well with the analytical calculations in [1].

Table 1: Electric and magnetic field information, at focal point, in air and inside focusing lens

Field information	Value
Peak electric field in air	$E_{\max}^{\text{NL}} = 6.247 \text{ (V/m)}$
Peak magnetic field in air	$H_{\max}^{\text{NL}} = 0.0151 \text{ (A/m)}$
Peak electric field inside lens	$E_{\max}^{\text{WL}} = 10.725 \text{ (V/m)}$
Peak magnetic field inside lens	$H_{\max}^{\text{WL}} = 0.0734 \text{ (A/m)}$
Impedance without lens	$Z_{\text{NL}} = E_{\max}^{\text{NL}}/H_{\max}^{\text{NL}} = 412.836 \ \Omega$
Impedance inside lens	$Z_{\text{WL}} = E_{\max}^{\text{WL}}/H_{\max}^{\text{WL}} = 146.139 \ \Omega$
Electric enhancement	$E_{\max}^{\text{WL}}/E_{\max}^{\text{NL}} = 1.717$
Magnetic enhancement	$H_{\max}^{\text{WL}}/H_{\max}^{\text{NL}} = 4.850$

3.3 Beam width comparison

Figure 3.3(a) compares the peak electric fields obtained, at the distances mentioned in section 2.2, in air and in the lens¹. As expected, the peak electric fields inside the lens are much higher. The beam width in air is much broader as a consequence of conservation of energy. Figure 3.3(b) shows a similar comparison of the peak magnetic fields. The impedance, at the focal point, i.e., E/H at $x=0$ cm, in air is $Z_{\text{NL}} = 6.247/0.0151 = 412.836 \ \Omega$, which is in approximate agreement with values obtained from experiments [5]. Inside the lens, $Z_{\text{WL}} = 10.725/0.0734 = 146.139 \ \Omega$.

For the curves shown in Fig. 3.3, the half-power width or beam width (or spot size) is $F_{\max}/\sqrt{2}$, where F corresponds to the peak electric or peak magnetic field at the focal point ($x = 0$ cm). The spot sizes are tabulated in table 2.

Table 2: Spot size of E and H field with and without the focusing lens and slab

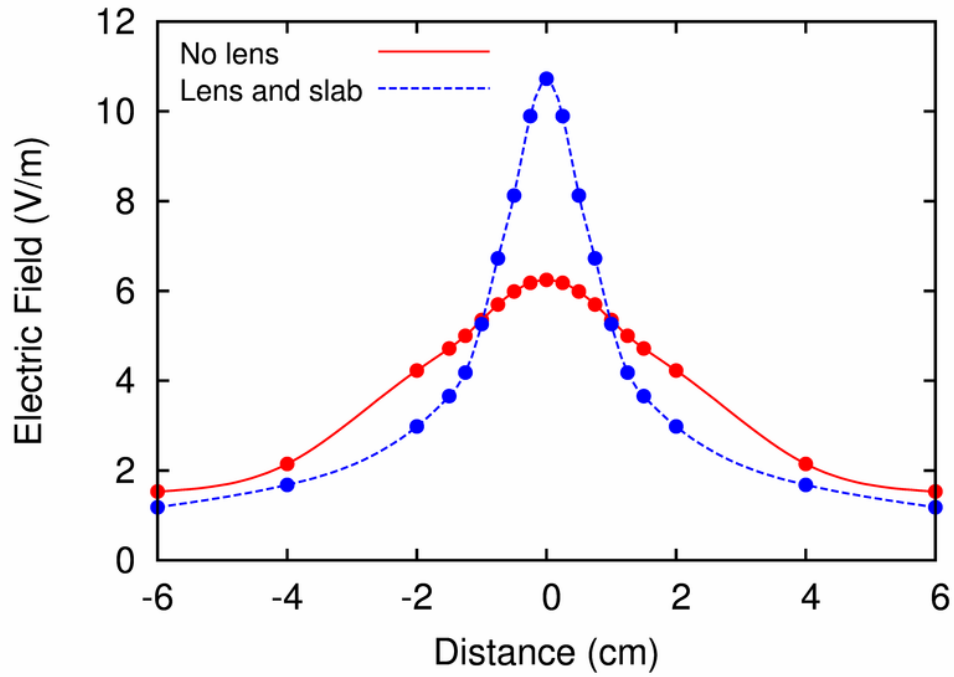
Field information	Spot diameter ($F_{\max}/\sqrt{2}$) from Fig. 3.3 in cm
E-Field No Lens	$\text{EFSS}_{\text{NL}} = 3.6104$
H-Field No Lens	$\text{HFSS}_{\text{NL}} = 3.6502$
E-Field With Lens	$\text{EFSS}_{\text{WL}} = 1.187$
H-Field With Lens	$\text{HFSS}_{\text{WL}} = 1.1954$

$$\text{Spot size ratio of electric field} \quad : \quad \text{EFSS}_{\text{NL}}/\text{EFSS}_{\text{WL}} \quad = \quad 3.6104/1.187 = 3.042$$

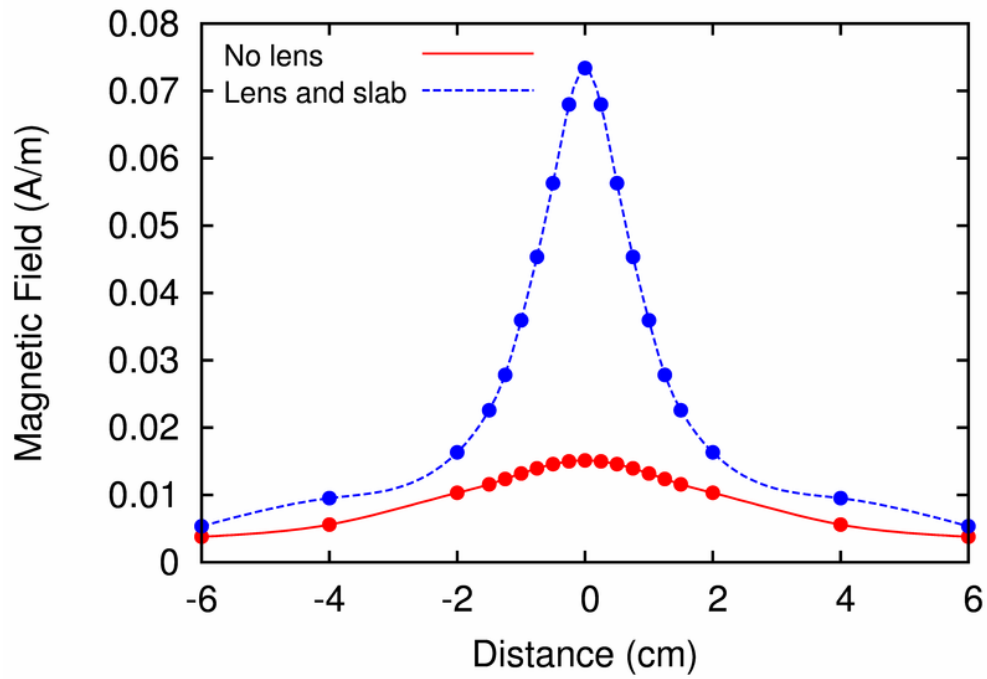
$$\text{Spot size ratio of magnetic field} \quad : \quad \text{HFSS}_{\text{NL}}/\text{HFSS}_{\text{WL}} \quad = \quad 3.6502/1.1954 = 3.053$$

The theoretical analysis in [6] leads to a definition of beam width (spot size) in terms of the pulse width in the Ψ direction, i.e., t_{Ψ} . Consequently, the spot sizes estimated in [1] cannot be compared to the simulation results. From table 2, the ratio of the electric field spot size in air and inside the lens is $\text{EFSS}_{\text{NL}}/\text{EFSS}_{\text{WL}} = 3.6104/1.187 = 3.042 \approx \sqrt{\epsilon_r} = \sqrt{9.0}$. For the magnetic field, $\text{HFSS}_{\text{NL}}/\text{HFSS}_{\text{WL}} = 3.6502/1.1954 = 3.054 \approx 3.0$.

¹Henceforth, “lens” will be used to refer to the focusing lens and the slab as a single unit.



(a) Peak electric field profile versus distance along x (see Fig. 2.1 for coordinate system), i.e., transverse through the focal point.



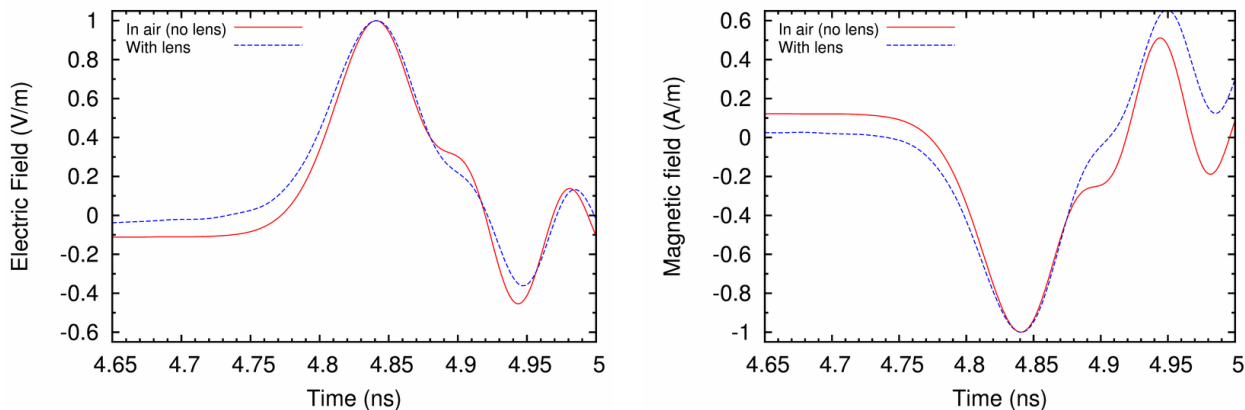
(b) Peak magnetic field profile versus distance x (see Fig. 2.1 for coordinate system), i.e., transverse through the focal point.

Figure 3.3: Peak electric and magnetic field profiles with and without the focusing lens and slab transverse through the focal point.

3.4 More observations on the focal waveform

3.4.1 Comparison of pulse widths

A comparison of the impulse pulse-widths in air and inside the lens could provide insight into factors, such as geometrical dispersion, that might have not been taken into account analytically. Since the lens and slab materials are assumed lossless and dispersionless in the simulations, the pulse widths are expected to be the same in both cases. Figure 3.4 compares the impulse pulse-widths for the electric and magnetic fields. As observed, the impulse responses are almost identical for the electrical and magnetic field. The simulations seem to indicate that any pulse broadening observed in experimental results should be due to (1) the sensor or (2) loss and dispersion in the focusing lens materials.



(a) Comparison of impulse pulse-width for electric field (b) Comparison of impulse pulse-width for magnetic field

Figure 3.4: Comparison of impulse pulse-widths for the electric and magnetic field

Note: The electric and magnetic enhancement factors in table 1 were obtained by taking the ratio of the impulse amplitudes in air and inside the lens. This was valid since, as seen above, the half-widths of the impulse in air and inside the lens are almost identical, i.e., 100 ps. If this were not the case, the electric and magnetic enhancements would be given by the ratio of the areas under the impulse curves, in air and in the lens (low-frequency pass filter).

3.4.2 Determination of input rise time from responses

The response at the focal point consists of the pre-pulse, impulse and post-pulse. The pre-pulse travels directly to the focal point without any interaction with the reflector. Thus, the rise time of the pre-pulse should mimic that of the source, which, in the simulation, is 100 ps. The impulse is the spherical wave from the source that is differentiated by the prolate-spheroidal reflector. Integrating the impulse should give the source input. In the presence of a lens, the pre-pulse is dispersed. The integrated impulse, however, should contain the source waveform information.

In Fig. 3.5 the normalized pre-pulse and impulse in air, and normalized impulse inside the lens, are compared to the input excitation in the simulation. The pre-pulse does not overlap with the input excitation. This is most likely due to lack of resolution in the simulation. The higher

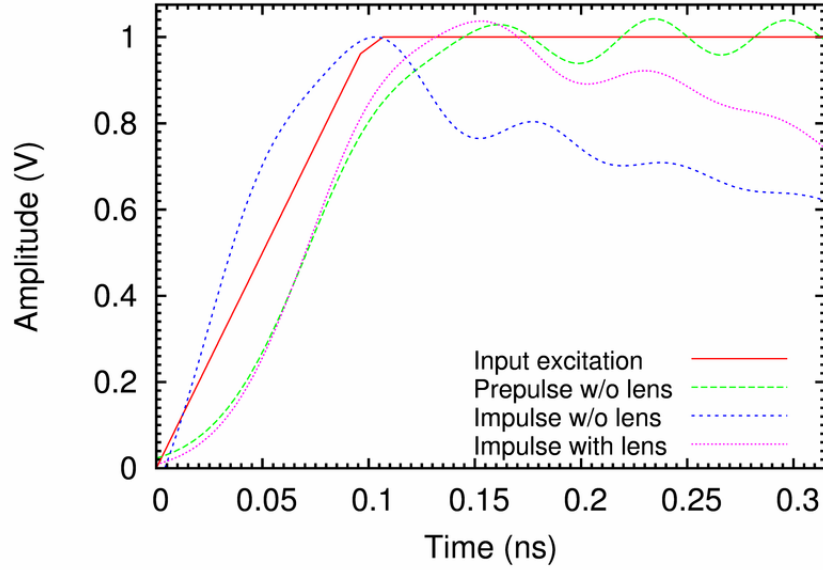


Figure 3.5: 3-D view of maximum electric field at second focal point

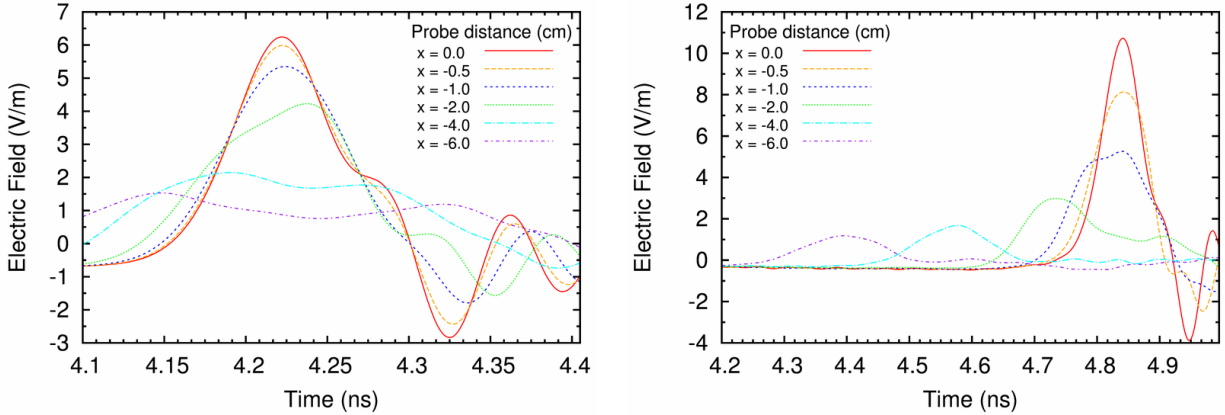
frequencies (< 100 ps or > 10 GHz) in the source excitation cannot be resolved. This results in the inability of the impulse to mimic the source waveform. The integrated impulse without lens is seen to follow the source excitation closely. The reason for this is not clear in light of the fact that the pre-pulse deviates so sharply from the input waveform. The integrated impulse inside the lens follows the pre-pulse without the lens. Again, this is believed to be from the numerical dispersion in the software.

- Numerical dispersion as a cause for discrepancies observed in the results above is only speculation and needs to be verified more rigorously. It is possible, though not likely, the waveforms of the pre-pulse and integrated impulse inside the lens do not follow the input closely due to other factors in the simulation. One possible method to verify numerical dispersion is to monitor the pre-pulse from source to the focal point in the simulations. This would give an indication of the deviation in rise time (if any).
- Another possible cause for discrepancies observed in Fig. 3.5 could be the finite gap between the feed-arms, 1 mm, used to source the excitation. This may lead to different propagation times of the rays originating from the source.
- The better agreement of the integrated impulse without the lens also needs to be explained. Why is this agreement better if the, much simpler and more direct, impulse waveform cannot be resolved by the software?

3.4.3 Responses at different distances from the focal point

It is observed that the maximum electric field in the impulse responses from probes located along the x -axis occur at distinctly different times. This is of course due to the spatially different location of each probe along the x -axis. The impulse responses for the electric field, in air and inside the

focusing lens, are shown in Fig. 3.6.



(a) Impulse responses of the electric field with no lens (b) Impulse responses of the electric field with focusing lens and slab for various probe locations.

Figure 3.6: Impulse responses in electric field with and without focusing lens for various probe locations along x (see Fig. 2.1 for coordinate system), i.e., transverse through the focal point.

Perhaps the most important observation in 3.6 is that the area under all the impulse responses is conserved.

4 Conclusions

1. The beam widths in air and inside the lens are close to those obtained by approximate analytical calculations. The ratios of the spot sizes, ratios of field maxima and impedances are also as estimated.
2. The pre-pulse is dispersed by the focusing lens and slab. Reflections from the slab are observed in the pre-pulse. A negative area in the post-pulse response is observed due to the filtering of lower frequencies by the focusing lens and slab.
3. The pulse width of the electric field impulse in air and inside the lens is almost the same.
4. It is not possible to verify the rise time from the electric field responses in air and with the lens. This is most likely because of numerical dispersion in the software used, although this needs to be more rigorously verified.

Two Arm Results

For comparison, the numerical simulation results for the 90° two arm case are summarized in table 3 and table 5.

Table 3: Electric and magnetic field information, at focal point, in air and with focusing lens

Field information	Value
Peak electric field in air	$E_{\max}^{\text{NL}} = 4.131 \text{ (V/m)}$
Peak magnetic field in air	$H_{\max}^{\text{NL}} = 0.0102 \text{ (A/m)}$
Peak electric field inside lens	$E_{\max}^{\text{WL}} = 6.836 \text{ (V/m)}$
Peak magnetic field inside lens	$H_{\max}^{\text{WL}} = 0.04788 \text{ (A/m)}$
Impedance in air	$Z_{\text{NL}} = E_{\max}^{\text{NL}}/H_{\max}^{\text{NL}} = 404.183 \ \Omega$
Impedance inside lens	$Z_{\text{WL}} = E_{\max}^{\text{WL}}/H_{\max}^{\text{WL}} = 142.738 \ \Omega$
Electric enhancement	$E_{\max}^{\text{WL}}/E_{\max}^{\text{NL}} = 1.65$
Magnetic enhancement	$H_{\max}^{\text{WL}}/H_{\max}^{\text{NL}} = 4.685$

Table 5: Spot size of E and H field with and without the focusing lens and slab

Field information	Spot size ($F_{\max}/\sqrt{2}$) from Fig. 3.3 in cm
E-Field No Lens	$EFSS_{\text{NL}} = 4.6554$
H-Field No Lens	$HFSS_{\text{NL}} = 4.9912$
E-Field With Lens	$EFSS_{\text{WL}} = 1.5134$
H-Field With Lens	$HFSS_{\text{WL}} = 1.5852$

$$\begin{aligned} \text{Spot size ratio of electric field} & : EFSS_{\text{NL}}/EFSS_{\text{WL}} = 4.6554/1.5134 = 3.0761 \\ \text{Spot size ratio of magnetic field} & : HFSS_{\text{NL}}/HFSS_{\text{WL}} = 4.9912/1.5852 = 3.149 \end{aligned}$$

References

- [1] C. E. Baum, S. Altunc, and P. Kumar, "Scaling relationships for electromagnetic parameters for focusing graded dielectric lenses," *Sensor and Simulation Note 537*, April 2009.
- [2] C. E. Baum, "Addition of a Lens Before the Second Focus of a Prolate-Spheroidal IRA," *Sensor and Simulation Note 512*, April 2006.

- [3] J. S. Tyo, "Optimization of the feed impedance for an arbitrary crossed-feed-arm impulse radiating antenna," *Sensor and Simulation Note 438*, November 1999.
- [4] M. J. Baretela and J. S. Tyo, "Improvement of prompt radiated response from impulse radiating antennas by aperature trimming," *IEEE Trans. Antennas Propagat.*, pp. 2158 – 2167, 2003.
- [5] S. Altunc, *Focal Waveform of a Prolate-Spheroidal Impulse Radiating Antenna (IRA)*. PhD thesis, University of New Mexico, December 2007.
- [6] C. E. Baum, "Focal waveform of a prolate-spheroidal impulse-radiating antenna," *Radio Science*, vol. 42, pp. 1–11, 2007.